AIMS Mathematics, 10(10): 24779–24803.
DOI: 10.3934/math.20251098
Received: 21 September 2025
Revised: 20 October 2025
Accepted: 24 October 2025
Published: 29 October 2025

https://www.aimspress.com/journal/Math

Research article

Impact of whitefly maturation on mosaic disease dynamics using a stage-structured model

Aeshah A. Raezah[1], **Konstantin B. Blyuss**[2,*], **Selim Reja**[3] **and Fahad Al Basir**[4,*]

[1] Department of Mathematics, Faculty of Science, King Khalid University, Abha 62529, Saudi Arabia
[2] Department of Mathematics, University of Sussex Falmer, Brighton BN1 9QH, United Kingdom
[3] Agricultural and Ecological Research Unit, Indian Statistical Institute, Kolkata 700108, India
[4] Department of Mathematics, Asansol Girls' College, Dr. Anjali Roy Sarani, Asansol-4, West Bengal 713304, India

* **Correspondence:** Email: K.Blyuss@sussex.ac.uk; fahadbasir@gmail.com.

Abstract: Plant viral infections are primarily propagated by adult insect vectors, which generally require a maturation period of approximately ten to twelve days. Following ingestion of the virus from an infected host plant, these vectors become capable of transmitting the pathogen to susceptible plants. In this study, a stage-structured mathematical model was formulated and analyzed to characterize the transmission dynamics of plant viral diseases mediated by adult insect vectors. Particular emphasis was placed on assessing how the maturation period of vectors influences the progression of infection transmission. To establish the mathematical validity of the model, it was shown to possess non-negative and bounded solutions, which confirms its well-posedness. We identified all steady states and studied their stability. The results show how infection rate, maturation rate, and maturation time can cause stability changes in steady states. Numerical stability and simulations were presented to analyze the behaviors of the system in different dynamical regimes. The stabilizing effect of the maturation period can help develop control methods for the management of plant viral diseases.

Keywords: vector-borne plant disease; basic reproduction number; stability analysis; sensitivity analysis; Hopf bifurcation; numerical simulation
Mathematics Subject Classification: 92-10, 37G15

1. Introduction

The majority of plant-infecting viruses depend on vectors for transmission to their host plants. The characteristics of these interactions, including duration and specificity, differ across virus-vector

systems [1]. Structural proteins encoded in plant viral genomes are critical for transmission, since they are expressed on the virions' surface [2]. Viral particles may be linked to specific sites in or on vectors by non-structural helper proteins, allowing viruses to bind to these sites until they are transmitted to their plants [3].

Among the known plant vectors, whiteflies are the vectors responsible for the transmission of around 120 different plant virus species [4–6]. For instance, Trialeurodes vaporariorum and T. abutilonia are documented to transmit as many as 111 viral species, whereas Bemisia tabaci is linked to the transmission of just three species. Both B. tabaci and T. vaporariorum are present in the European-Mediterranean region; however, the distribution of B. tabaci seems to be rather limited. Begomovirus is the dominant genus among whitefly-transmitted viruses, accounting for nearly 90% of recorded cases. Crinivirus represents about 6%, while the remaining 4% are distributed among the Closterovirus, Ipomovirus, and Carlavirus genera [7]. Due to their extensive presence in warm regions and capacity to infest both herbaceous and woody plants, whiteflies are regarded as not only detrimental agricultural pests but also pivotal agents in the epidemiology of plant viral diseases [8].

Vectors have a hemimetabolous life cycle consisting of three primary phases: Egg, nymph, and adult [9, 10]. Fusiform eggs are oviposited on the abaxial surface of the leaf, where they undergo embryonic development and hatch into nymphs within 3 to 10 days. The motile nymphs of the first instar settle on a particular plant. They develop a puparium following three molts, and the adult emerges two to six days later. The disease is constantly spread by motile adults [11]. Mature vectors are piercing-sucking adults that feed by piercing their stylets into plants like aphids. They multiply easily in a glasshouse, and as the temperature and plant size increase, the spread of vectors increases. Adults are the main carriers of the virus due to their mobility and wings, and while they can develop midgut infections from feeding on sap of infected plants, immature insects cannot spread the virus. Glasshouse summer conditions and moderate temperatures are ideal for these insects. Whitefly vectors need twelve to twenty days to mature [7]. When modeling plant disease spread by these vectors, the maturation time has to be taken into account, as it can affect the rate at which the disease spreads, and it can also cause stability switches. In fact, including time delays in similar ecological models is known to result in a plethora of dynamic behaviors, including oscillations and bifurcations of different types, as well as stability and instability developing [12, 13] or disappearing [14, 15].

Adult whiteflies carry plant viruses during feeding, which can spread the virus to new plants after a 24-hour acquisition access period. This can result in mosaic diseases, such as cassava mosaic disease and Jatropha mosaic disease [16, 17]. Understanding the transmission dynamics of these diseases can be aided by mathematical modeling using ordinary differential equations [18], or using delay differential equations [19, 20]. One of the first-ever delay differential equation models for plant epidemics was introduced by Van der Planck [21], and a discrete-time approximation of that model was studied later [22]. The majority of time-delayed models concentrate on determining thresholds for delay-induced instability and subsequent emergence or disappearance of oscillatory solutions [23, 24]. At the same time, it is important to also pay attention to the specific biological mechanism behind time delays in such models, as they can lead to unexpected and, at times, deceptive conclusions [14, 15].

Al Basir et al. [15] developed a delayed model to capture the impact of whitefly maturation time on mosaic disease of cassava, while a model for mosaic disease of Jatropha was studied in [25]. Al Basir [26] studied the role of the maturation period of the whitefly vector in the mosaic disease of *Jatropha c.* by including a time delay in the infection transmission term $\lambda sv(t-\tau)$ to represent the fact

that only mature vectors can transmit the virus. Adhurya et al. [27] analyzed a stage-structured model for plant-whitefly vector interactions, in which the population of whiteflies was divided into immature whiteflies and adults, which were further subdivided into susceptible and infective compartments. The population of immature vectors was assumed to grow linearly, while in [25] the authors assumed logistic growth for vector populations, but did not consider different vector stages. In this paper, we modify the multi-stage model of Adhurya et al. [27] to include logistic growth of immature vectors, while also accounting for the maturation period that is required for these immature vectors to become adults. The main focus is on exploring how the maturation period can affect the dynamics and stability of different steady states.

Here, our consideration has been the logistic-type growth of the immature whitefly vectors to develop the mathematical model proposed in [27]. Moreover, we have incorporated a time delay due to the maturation period of immature vectors in the proposed model. It is well known that only mature vectors can carry the mosaic virus. We have analyzed the proposed delay model using qualitative theory to understand the dynamics of the system, such as the stability switch of the steady states and bifurcations. Thus, the main aim of this research is to study the impact of the vector's maturation period on the disease transmission, using a stage-structured model where immature vectors follow logistic growth. We have analyzed the dynamics of the system with and without delay analytically as well as numerically to study the dynamics of the disease.

The remaining parts of this paper are organized as follows. Section 2 introduces the mathematical model for plant virus dynamics accounting for vector maturation delay and establishes its well-posedness. Section 3 presents a rigorous analytical study of the existence and stability of the steady states, while Section 4 provides the sensitivity analysis of the model parameters. The outcome of the numerical simulations are presented in Section 5. Concluding remarks and potential avenues for future investigation are discussed in Section 6.

2. The mathematical model

To analyze the effects of time-delayed dynamics of plant viruses in the presence of multiple stages in the vector population, we follow an earlier model proposed in [27], subject to some additional assumptions. The detailed derivation is mentioned below.

We consider the plant population being divided into susceptible, $s(t)$, and infected plants, $w(t)$. The virus is not modeled explicitly but rather is taken to be represented by the infective whitefly vectors, like earlier models of plant virus infections [8, 25, 28].

The total vector population is categorized into immature vectors, denoted by $v_1(t)$, and mature vectors. The mature class is further partitioned into non-infective vectors $v_2(t)$ and infective vectors $v_3(t)$.

Mature vectors can produce offspring, resulting in the emergence of new immature vectors, whose growth is limited, however, by the carrying capacity, which is represented by the total biomass of plants (both susceptible and infected). The virus cannot be transmitted vertically between vectors, nor can it be transmitted directly from one vector to another. Furthermore, the virus neither induces mortality nor triggers disease symptoms in its vector hosts [25, 28]. Once infected, a vector remains capable of transmission throughout its lifespan.

We consider the susceptible plant population, denoted by $s(t)$, to follow logistic growth

characterized by a linear growth rate r and a carrying capacity K, which reflects the spatial limitations of the plantation. Transmission of infection occurs when infected mature vectors $v_3(t)$ feed on susceptible plants, leading to their conversion into infected plants $w(t)$ at a rate λ. Conversely, mature non-infective vectors $v_2(t)$ become infective upon feeding on infected plants, acquiring the virus at a rate β and transitioning into the infective class $v_3(t)$.

The population of immature vectors $v_1(t)$ is assumed to grow at rate b proportionally to the number of mature vectors, irrespective of their infection status. The vectors are merely the carriers of disease to and from plants, but the disease does not directly affect them. We assume that all vector populations die at a constant rate c. Infected plants have a natural mortality and a disease-induced mortality. We assume a total mortality rate α.

Under the assumption that plants, both susceptible and infected, can simultaneously support up to a number of vectors, the overall carrying capacity for vectors, as provided by plants, is given by $a(s + w)$. Accordingly, the temporal evolution of the immature vector population is governed by the following equation:

$$\frac{dv_1}{dt} = b(v_2 + v_3)\left[1 - \frac{v_1 + v_2 + v_3}{a(s + w)}\right] - mv_1 - cv_1, \tag{1}$$

where m is the vector maturation rate. Considering $\tau \in \mathbb{R}_+$ to be the maturation time taken by immature vectors to mature, the influx of new mature vectors at time t is represented by the term $me^{-c\tau}v_1(t - \tau)$, where $v_1(t - \tau)$ is the population of immature vectors at time $(t - \tau)$, and the multiplication factor $e^{-c\tau}$ represents the survival probability of inoculum through the period of maturation $[t - \tau, t]$, with c being the above-mentioned natural death rate of vectors.

Based on the preceding assumptions, the governing mathematical model is formulated as follows:

$$\begin{aligned}
\frac{ds}{dt} &= rs\left[1 - \frac{s + w}{K}\right] - \lambda s v_3,\\
\frac{dw}{dt} &= \lambda s v_3 - \alpha w,\\
\frac{dv_1}{dt} &= b(v_2 + v_3)\left[1 - \frac{v_1 + v_2 + v_3}{a(s + w)}\right] - mv_1 - cv_1,\\
\frac{dv_2}{dt} &= me^{-c\tau}v_1(t - \tau) - \beta v_2 w - cv_2,\\
\frac{dv_3}{dt} &= \beta v_2 w - cv_3,
\end{aligned} \tag{2}$$

with initial population sizes

$$\begin{aligned}
&s(0) > 0, \quad w(0) > 0, \quad s(0) + w(0) \le K, \quad v_2(0) \ge 0, \quad v_3(0) \ge 0,\\
&v_1(\omega) = \phi(\omega) \ge 0, \quad \omega \in [-\tau, 0], \quad 0 < v_1(0) \le \frac{abK}{4(m + c)},\\
&v_2(0) + v_3(0) \le a[s(0) + w(0)], \quad v_2(0) + v_3(0) \le \frac{me^{-c\tau}abK}{4c(m + c)}.
\end{aligned} \tag{3}$$

Prior to undertaking the dynamics analysis, we establish the well-posedness of the model.

Theorem 1. *All solutions of model (2) satisfying initial conditions (3) and the condition* $v_2(t) + v_3(t) \leq a[s(t) + w(t)]$ *will remain non-negative for all* $t \geq 0$ *and ultimately bounded in the positively invariant region*

$$\mathcal{G} = \left\{(s, w, v_1, v_2, v_3) \in \mathbb{R}^5_+ : 0 < s + w \leq K, \quad 0 \leq v_1 \leq V_1, \quad 0 \leq v_2 + v_3 \leq V_{23}\right\}, \tag{4}$$

where $V_1 = \dfrac{abK}{4(m + c)}$ *and* $V_{23} = \dfrac{me^{-c\tau}abK}{4c(m + c)}$.

Proof. As a first step, we establish non-negativity of all variables in model (2). Evaluating ds/dt when $s = 0$ yields $ds/dt = 0$, indicating that with $s(0) > 0$, we have $s(t) \geq 0$ for all $t \geq 0$. To make further progress, rather than considering the entire real half-axis $t \geq 0$, we focus on a single time interval $[0, \tau]$. Considering the equation for v_2 over this time interval, we find

$$\left.\frac{dv_2}{dt}\right|_{v_2=0} = me^{-c\tau}v_1(t - \tau) = me^{-c\tau}\phi(t - \tau) \geq 0,$$

where we have used the initial condition for v_1 over the interval $[-\tau, 0]$. This shows that v_2 cannot become negative for t in $[0, \tau]$. Next, we consider a subsystem of equations for w and v_3, for which we note that the derivatives of w and v_3 at the boundaries $w = 0$ and $v_3 = 0$ are, respectively, $\left.\dfrac{dw}{dt}\right|_{w=0} = \lambda s v_3$ and $\left.\dfrac{dv_3}{dt}\right|_{v_3=0} = \beta v_2 w$. Since we have just shown that $s(t) \geq 0$ and $v_2(t) \geq 0$, the source terms for w and v_3 are non-negative when evaluated on their respective boundaries. Due to this cooperative structure, where the inflow to one compartment is positively coupled to the size of the other, the solutions $w(t)$ and $v_3(t)$ remain non-negative for all t in the time interval $[0, \tau]$ we are considering.

Having established non-negativity of $s(t)$ and $w(t)$, now we want to show that a stricter condition holds, namely, that $s(t) + w(t) > 0$, which is essential for the feasibility of the equation for v_1 that contains the term $a(s + w)$ in the denominator of the fraction in the logistic term. Introducing a new variable $P(t) = s(t) + w(t)$ and adding equations for s and w, we obtain

$$\frac{dP}{dt} = rs\left(1 - \frac{P}{K}\right) - \alpha w.$$

Focusing on very small, but positive, values of P, we then have

$$\frac{dP}{dt} = rs\left(1 - \frac{P}{K}\right) - \alpha w \geq -\alpha w \geq -\alpha P.$$

A comparison principle then suggests that the solution $P(t)$ is bounded below by the solution of $dx/dt = -\alpha x$, which is $x(t) = P(0)e^{-\alpha t}$, and hence, $P(t) \geq P(0)e^{-\alpha t} > 0$ for all finite $t \geq 0$. Therefore, $s(t) + w(t) > 0$ for all $t \geq 0$, ensuring the denominator $a(s + w)$ is always well-defined.

Finally, we look at the equation for v_1, which, when evaluated at $v_1 = 0$, reduces to

$$\frac{dv_1}{dt} = b(v_2 + v_3)\left(1 - \frac{(v_2 + v_3)}{a(s + w)}\right).$$

As we have already established that $v_2(t) \geq 0$ and $v_3(t) \geq 0$, while $s(t) + w(t) > 0$, in light of the condition $v_2(t) + v_3(t) < a[s(t) + w(t)]$ required in the theorem, we obtain $\dfrac{dv_1}{dt} \geq 0$, which shows that

$v_1(t) \geq 0$. Now that we have proven non-negativity of all state variables on the interval $[0, \tau]$, together with an extra condition $(s(t) + w(t)) > 0$, the same procedure can be repeated for the interval $[\tau, 2\tau]$ and others, thus showing that all solutions of model (2) remain non-negative with $(s(t) + w(t)) > 0$ for all $t \geq 0$.

The next step is to prove the boundedness of all variables. Considering $P(t) = s(t) + w(t)$, we have

$$\frac{dP}{dt} = rs\left(1 - \frac{P}{K}\right) - \alpha w.$$

Given the initial condition $P(0) = s(0) + w(0) \leq K$, let us consider a situation when $P(t) = K$. In this case, we have

$$\frac{dP}{dt} = -\alpha w \leq 0,$$

indicating that $P(t)$ cannot exceed the value of $P = K$. In other words, $s(t) + w(t) \leq K$ for all $t \geq 0$.

Non-negativity of $v_1(t)$ and $s(t) + w(t) \leq K$ allow one to write

$$\frac{dv_1}{dt} = b(v_2 + v_3)\left(1 - \frac{(v_1 + v_2 + v_3)}{a(s + w)}\right) - (m + c)v_1 \leq b(v_2 + v_3)\left(1 - \frac{(v_2 + v_3)}{aK}\right) - (m + c)v_1.$$

Using the fact that the quadratic function $bx\left(1 - \dfrac{x}{C}\right)$ has a maximum value of $bC/4$, we obtain

$$\frac{dv_1}{dt} \leq \frac{abK}{4} - (m + c)v_1,$$

and the comparison principle shows that with the initial condition $0 < v_1(0) < V_1$ as in (3), we then have $0 \leq v_1(t) \leq V_1 = \dfrac{abK}{4(m + c)}$ for all $t \geq 0$.

The dynamics of $U(t) = v_2(t) + v_3(t)$ are described by the following equation,

$$\frac{dU}{dt} = me^{-c\tau}v_1(t - \tau) - cU. \tag{5}$$

Using the bound $v_1 \leq V_1$, we now have

$$\frac{dU}{dt} \leq \frac{me^{-c\tau}abK}{4(m + c)} - cU, \tag{6}$$

and hence, with $U(0) \leq V_{23} = \dfrac{me^{-c\tau}abK}{4c(m + c)}$, we have $U(t) = v_2(t) + v_3(t) \leq V_{23}$ for all $t \geq 0$, which completes the proof. □

3. Steady states and their stability

System (2) may possess at most three steady states, given by:
(i) the vector-free steady state, $\mathcal{U}_1(K, 0, 0, 0, 0)$;
(ii) the disease-free steady state, $\mathcal{U}_2(K, 0, \bar{v}_1, \bar{v}_2, 0)$, with

$$\bar{v}_1 = \frac{c\bar{v}_2}{\varpi}, \quad \bar{v}_2 = \frac{aK[b\varpi - c(m + c)]}{b(c + \varpi)}, \tag{7}$$

where $\varpi = me^{-c\tau}$. $\mathcal{U}_2$ is biologically feasible only when

$$b\varpi - c(m + c) > 0; \tag{8}$$

(iii) the endemic steady state, $\mathcal{U}^* = (s^*,\ w^*,\ v_1^*,\ v_2^*,\ v_3^*)$, where

$$s^* = \frac{\alpha K(r - \lambda v_3^*)}{r(\lambda v_3^* + \alpha)}, \quad w^* = \frac{\lambda s^* v_3^*}{\alpha}, \quad v_1^* = \frac{c[\beta\lambda v_3^* s^* - \alpha c]}{\lambda\beta m e^{-c\tau} s^*}, \quad v_2^* = \frac{c\alpha}{\lambda\beta s^*}, \tag{9}$$

and v_3^* is the positive root of the quartic equation

$$l_4 v^4 + l_3 v^3 + l_2 v^2 + l_1 v + l_0 = 0, \tag{10}$$

with coefficients

$$\begin{aligned}
l_4 &= K^2 b\beta^2\lambda^4\varpi(r + Ka\lambda),\\
l_3 &= K^2 a\beta^2 c^2\lambda^4(r - K\lambda) - 2K^2 b\beta^2\lambda^3\varpi r^2 - K^3 a\beta^2 c\lambda^5 m - Kb\beta^2 c\lambda^3 r^2\\
&\quad + K^2 b\beta^2 c\lambda^4 r - 3K^3 ab\beta^2\lambda^4\varpi r + K^2 a\beta^2 c\lambda^4 mr - 2Kb\beta c\lambda^3\varpi r^2 - K^2 ab\beta c\lambda^4\varpi r,\\
l_2 &= bc^2\lambda^2 r^3(\beta + \varpi) + 3K^3 a\beta^2 c^2\lambda^4 r - 2K^2 b\beta^2 c\lambda^3 r^2 + K^2 b\beta\lambda^2 r(\varpi r^2 - a\alpha c\lambda\varpi)\\
&\quad + K\lambda^2\beta c(-2Ka\beta c\lambda r^2 - bc\lambda r^2 + b\beta c\lambda r^3 - \alpha b\beta\lambda r^2 + 3K^2 a\beta\lambda^2 mr + Ka\alpha\beta c\lambda^2 r)\\
&\quad + 3K^3 ab\beta^2\lambda^3\varpi r^2 - 2K^2 a\beta^2 c\lambda^3 mr^2 + 2Kb\beta c\lambda^2\varpi r^3 - 2K\alpha b\beta c\lambda^2\varpi r^2\\
&\quad + K^2 a\alpha\beta^2 c\lambda^3 mr + 2K^2 ab\beta c\lambda^3\varpi r^2,\\
l_1 &= K^2 a\beta^2\lambda^2 r^2 c^2(r - 3K\lambda) + 2\alpha bc^2\lambda\varpi r^3 + Kb\beta c^2\lambda^2 r^3 + K^2 b\beta^2 c\lambda^2 r^3 + 2\alpha b\beta c^2\lambda r^3\\
&\quad - K^3 ab\beta^2\lambda^2\varpi r^3 + K^2 a\beta^2 c\lambda^2 mr^3 - 3K^3 a\beta^2 c\lambda^3 mr^2 + K\alpha b\beta^2 c\lambda r^3 - 2K^2 a\alpha\beta^2 c^2\lambda^2 r^2\\
&\quad - K\alpha b\beta c^2\lambda^2 r^2 - K^2 ab\beta c\lambda^2\varpi r^3 + 2K\alpha b\beta c\lambda\varpi r^3 - 2K^2 a\alpha\beta^2 c\lambda^2 mr^2 + 2K^2 a\alpha b\beta c\lambda^2\varpi r^2,\\
l_0 &= \alpha^2 b\beta c^2 r^3 + \alpha^2 bc^2\varpi r^3 + Kc(K^2 a\beta^2 c\lambda^2 r^3 + Ka\alpha\beta^2 c\lambda r^3 + K^2 a\beta^2\lambda^2 mr^3 + \alpha b\beta c\lambda r^3)\\
&\quad + K^2 a\alpha\beta c\lambda(m - b\varpi).
\end{aligned}$$

Since $l_4 > 0$, Eq (10) has at least one positive root if $l_0 < 0$.

3.1. Basic reproduction number

The basic reproduction number, denoted as $\mathcal{R}_0$, refers to the average number of new infections caused by one infected person in a fully susceptible population. To determine $\mathcal{R}_0$ for system (2), we employ the next-generation matrix method, following the framework described in [29]. This methodology entails defining two vector functions: $\mathcal{F}$, representing the rate at which new infections arise, and $\mathcal{V}$, describing the rate at which individuals exit the infected compartments. For the present model, these vectors take the form

$$\mathcal{F} = \begin{pmatrix} \lambda s v_3 \\ \beta v_2 w \end{pmatrix}, \quad \mathcal{V} = \begin{pmatrix} \alpha w \\ c v_3 \end{pmatrix}.$$

As a next step, we define matrices $\hat{\mathcal{F}} = \partial\mathcal{F}_i(\mathcal{U}_1)/\partial z_j$ and $\hat{\mathcal{V}} = \partial\mathcal{V}_i(\mathcal{U}_1)/\partial z_j$, where z_j are variables associated with the infected compartments, namely, w and v_3. Evaluating these matrices at the disease-free equilibrium $\mathcal{U}_1$, one obtains

$$\hat{\mathcal{F}} = \begin{pmatrix} 0 & \lambda K \\ \beta\bar{v}_2 & 0 \end{pmatrix}, \quad \hat{\mathcal{V}} = \begin{pmatrix} \alpha & 0 \\ 0 & c \end{pmatrix}.$$

According to [29], the basic reproduction number $\mathcal{R}_0$ is then given by

$$\mathcal{R}_0 = \rho(\hat{\mathcal{F}}\hat{\mathcal{V}}^{-1}),$$

where ρ is the spectral radius of the matrix

$$\hat{\mathcal{F}}\hat{\mathcal{V}}^{-1} = \frac{1}{c\alpha}\begin{pmatrix} 0 & \lambda\alpha K \\ c\beta\bar{v}_2 & 0 \end{pmatrix}.$$

Hence, $\mathcal{R}_0$ for the system (2) is expressed as

$$\mathcal{R}_0 = \sqrt{\frac{\lambda\beta K\bar{v}_2}{c\alpha}}.$$

Remark 1. *(i) The disease-free equilibrium $\mathcal{U}_2$ is feasible when $bme^{-c\tau} > c(m+c)$ holds. (ii) As long as the condition $l_4 < 0$ is satisfied, the existence of at least one endemic steady state is ensured. Extensive numerical calculations show that the endemic equilibrium exists for $\mathcal{R}_0 > 1$ and $\beta\lambda v_3^* s^* > \alpha c$, and it is unique when $s^* < K$.*

3.2. Linearized system and characteristic equation

To examine the stability of the distinct steady states of system (2), we linearize it near any steady state $\mathcal{U}(s, w, v_1, v_2, v_3)$ to obtain

$$\frac{dX}{dt} = GX(t) + HX(t-\tau), \tag{11}$$

where $G = [a_{ij}]$ and $H = [b_{ij}]$ are 5×5 matrices as given below:

$$G = \left[a_{ij}\right] = \begin{bmatrix} a_{11} & -\frac{rs}{K} & 0 & 0 & -\lambda s \\ \lambda v_3 & -\alpha & 0 & 0 & \lambda s \\ a_{31} & a_{32} & a_{33} & a_{34} & a_{35} \\ 0 & -\beta v_2 & 0 & -(\beta w + c) & 0 \\ 0 & \beta v_2 & 0 & \beta w & -c \end{bmatrix}, \quad H_{ij} = [b_{ij}] = \begin{bmatrix} 0 & 0 & 0 & 0 & 0 \\ 0 & 0 & 0 & 0 & 0 \\ 0 & 0 & 0 & 0 & 0 \\ 0 & 0 & me^{-c\tau} & 0 & 0 \\ 0 & 0 & 0 & 0 & 0 \end{bmatrix},$$

with

$$a_{11} = r\left(1 - \frac{2s+w}{K}\right) - \lambda v_3, \quad a_{35} = b\left(1 - \frac{v_1+v_2+2v_3}{a(s+w)}\right),$$

$$a_{31} = \frac{b(v_2+v_3)(v_1+v_2+v_3)}{a(s+w)^2}, \quad a_{32} = \frac{b(v_2+v_3)(v_1+v_2+v_3)}{a(s+w)^2},$$

$$a_{33} = -\frac{b(v_2+v_3)}{a(s+w)} - (m+c), \quad a_{34} = \quad b\left(1 - \frac{2v_2+v_1+v_3}{a(s+w)}\right).$$

At any equilibrium $\mathcal{U}(s, w, v_1, v_2, v_3)$, the characteristic equation can be obtained as

$$\psi(\xi, \tau) = \mid \xi I - G - e^{-\xi\tau} H \mid = 0,$$

which explicitly has the form

$$\psi(\xi, \tau) = \left(\xi^5 + \sigma_1\xi^4 + \sigma_2\xi^3 + \sigma_3\xi^2 + \sigma_4\xi + \sigma_5\right) + e^{-\xi\tau}\left(\sigma_6\xi^3 + \sigma_7\xi^2 + \sigma_8\xi + \sigma_9\right) = 0, \tag{12}$$

with the coefficients

$$\begin{aligned}
\sigma_1 &= -(a_{11} + a_{22} + a_{44} + a_{33} + a_{55}),\\
\sigma_2 &= a_{11}a_{22} - a_{12}a_{21} + a_{11}a_{33} + a_{22}a_{33} + a_{11}a_{44} + a_{22}a_{44} + a_{33}a_{44}\\
&\quad + a_{15}a_{52} + a_{11}a_{55} + a_{22}a_{55} + a_{33}a_{55} + a_{44}a_{55},\\
\sigma_3 &= a_{12}a_{21}a_{33} - a_{11}a_{22}a_{33} - a_{12}a_{21}a_{44} - a_{11}a_{22}a_{44} - a_{11}a_{33}a_{44} - a_{22}a_{33}a_{44}\\
&\quad - a_{11}a_{15}a_{52} - a_{15}a_{21}a_{52} - a_{15}a_{33}a_{52} - a_{15}a_{44}a_{52} + a_{15}a_{42}a_{54} + a_{12}a_{21}a_{55}\\
&\quad - a_{11}a_{22}a_{55} - a_{11}a_{33}a_{55} - a_{22}a_{33}a_{55} - a_{11}a_{44}a_{55} - a_{22}a_{44}a_{55} - a_{33}a_{44}a_{55},\\
\sigma_4 &= -a_{12}a_{21}a_{33}a_{44} + a_{11}a_{22}a_{33}a_{44} + a_{11}a_{15}a_{33}a_{52} + a_{15}a_{21}a_{33}a_{52} + a_{11}a_{15}a_{44}a_{52}\\
&\quad + a_{15}a_{21}a_{44}a_{52} + a_{15}a_{33}a_{44}a_{52} - a_{11}a_{15}a_{42}a_{54} - a_{15}a_{21}a_{42}a_{54} - a_{15}a_{33}a_{42}a_{54}\\
&\quad - a_{12}a_{21}a_{33}a_{55} + a_{11}a_{22}a_{33}a_{55} - a_{12}a_{21}a_{44}a_{55} + a_{11}a_{22}a_{44}a_{55}\\
&\quad + a_{11}a_{33}a_{44}a_{55} + a_{22}a_{33}a_{44}a_{55},\\
\sigma_5 &= -a_{11}a_{15}a_{33}a_{44}a_{52} - a_{15}a_{21}a_{33}a_{44}a_{52} + a_{11}a_{15}a_{33}a_{42}a_{54}\\
&\quad + a_{15}a_{21}a_{33}a_{42}a_{54} + a_{12}a_{21}a_{33}a_{44}a_{55} - a_{11}a_{22}a_{33}a_{44}a_{55},\\
\sigma_6 &= -a_{34}b_{43}, \quad \sigma_7 = a_{11}a_{34}b_{43} - a_{22}a_{34}b_{43} + a_{34}b_{43}a_{55},\\
\sigma_8 &= a_{12}a_{21}a_{34}b_{43} - a_{11}a_{22}a_{34}b_{43} - a_{15}a_{34}b_{43}a_{52}\\
&\quad - a_{15}a_{31}b_{43}a_{54} + a_{15}a_{32}b_{43}a_{54} - a_{11}a_{34}b_{43}a_{55} - a_{22}a_{34}b_{43}a_{55},\\
\sigma_9 &= a_{11}a_{15}a_{34}b_{43}a_{52} + a_{12}a_{15}a_{31}b_{43}a_{54} - a_{15}a_{21}a_{32}b_{43}a_{54} + a_{15}a_{22}a_{31}b_{43}a_{54}\\
&\quad - a_{11}a_{15}a_{32}b_{43}a_{54} + a_{11}a_{22}a_{34}b_{43}a_{55} - a_{12}a_{21}a_{34}b_{43}a_{55} + a_{15}a_{21}a_{34}b_{43}a_{52}.
\end{aligned}$$

3.3. Stability analysis of the vector-free and disease-free steady states

Evaluating the matrices G and H at the vector-free steady state $\mathcal{U}_1$, we see that the characteristic equation has three negative roots as $-r < 0$, $-c < 0$, and $-\alpha < 0$. The rest of the roots satisfy the following equation in ξ:

$$\xi^2 + (m + c + cK)\xi + c(m + c) - b\varpi = 0, \tag{13}$$

where the parameter $\varpi = me^{-c\tau}$ was introduced earlier. Provided the following condition,

$$b\varpi < c(m + c), \tag{14}$$

the vector-free equilibrium $\mathcal{U}_1$ is stable. In the case of the disease-free equilibrium point $\mathcal{U}_2$, we have

$$s = K, \ v_1 = \bar{v}_1, \ v_2 = \bar{v}_2,$$

where

$$\bar{v}_1 = \frac{c\bar{v}_2}{\varpi}, \quad \bar{v}_2 = \frac{aK[b\varpi - c(m + c)]}{b(c + \varpi)}.$$

This gives the coefficients of matrices G and H as

$$a_{11} = -r,\ a_{22} = -\alpha,\ a_{55} = -c,\ a_{25} = \lambda K,\ a_{52} = \beta\bar{v}_2,\ a_{33} = -\frac{b\bar{v}_2}{aK} - (m + c),$$

$$a_{44} = -c,\ a_{34} = b\left(1 - \frac{2\bar{v}_2 + \bar{v}_1}{aK}\right),\ b_{43} = me^{-c\tau}.$$

Hence, at $\mathcal{U}_2$, one eigenvalue is $-r < 0$, while the following characteristic equation determines the rest of the eigenvalues:

$$\left[\xi^2 - (a_{22} + a_{55})\xi - a_{25}a_{52} + a_{22}a_{55}\right] \times \left[\xi^2 - (a_{33} + a_{44})\xi + a_{33}a_{44} - a_{34}b_{43}e^{-\xi\tau}\right] = 0,$$

or explicitly,

$$\left[\xi^2 + (\alpha + c)\xi + c\alpha\left(1 - \mathcal{R}_0^2\right)\right] \times \left[\xi^2 + L_1\xi + L_2 - e^{-\xi\tau}L_3\right] = 0, \tag{15}$$

with

$$L_1 = \left[(m + c) + \frac{b\varpi - c(m + c)}{c + \varpi}\right]K + c, \qquad L_2 = c\left[(m + c) + \frac{b\varpi - c(m + c)}{c + \varpi}\right],$$

$$L_3 = b\varpi - \left(2b + \frac{bc}{\varpi}\right)\frac{b\varpi - c(m + c)}{c + \varpi}.$$

From the first bracket of the above equation, we conclude that the eigenvalues are negative when $\mathcal{R}_0 < 1$, and one of them goes through zero along the real axis at $\mathcal{R}_0 = 1$. The second bracket of Eq (15) is a transcendental equation in ξ,

$$\xi^2 + L_1\xi + L_2 - e^{-\xi\tau}L_3 = 0. \tag{16}$$

Prior to analyzing this equation, we note that for any value of $\tau \geq 0$, it immediately follows from the definitions of L_2 and L_3 that

$$L_2 - L_3 = b\varpi - c(m + c) > 0,$$

which is nothing else but the feasibility criteria of the disease-free equilibrium $\mathcal{U}_2$, and hence, it is always satisfied whenever that steady state is biologically feasible.

Case I. $\tau = 0$. The Eq (16) is a regular quadratic with two roots, which have negative real parts, provided

$$L_1 > 0,\ L_2 - L_3 > 0. \tag{17}$$

Both of these conditions are automatically satisfied whenever $\mathcal{U}_2$ is feasible.

Case II. $\tau > 0$. If we insert $\xi = \eta + i\kappa$ into Eq (16), and then separate the result into real and imaginary components, we obtain the following outcomes:

$$-\kappa^2 + \eta^2 + \eta L_1 + L_2 = e^{-\eta\tau}L_3\cos\kappa\tau,$$

$$2\eta\kappa + \kappa L_1 = e^{-\eta\tau}L_3\sin\kappa\tau.$$

By squaring each of the two equations and then adding them together, we obtain:

$$(\eta^2 + \kappa^2)^2 + \kappa^2c^2 + (\eta L_1 + L_2^2) + 2\eta(\kappa^2L_1 + \eta L_2) = e^{-2\eta\tau}L_3^2, \tag{18}$$

which can only be satisfied when $\eta < 0$, indicating that Eq (16) can only have roots with negative real parts.

To establish the result, we proceed by contradiction. Assume there exists a $\tau > 0$ such that $\xi = i\kappa$ is a purely imaginary solution to Eq (16). Under this assumption, Eq (18) simplifies to:

$$z^2 + c^2 z + (L_2^2 - L_3^2) = 0, \quad z = \kappa^2. \tag{19}$$

Given that $L_2^2 - L_3^2 > 0$, no positive real roots can be found for z. This implies that Eq (16) does not admit any purely imaginary roots.

These considerations can be summarized in the following result.

Theorem 2. *For model (2), if $\mathcal{R}_0 < 1$, then the disease-free steady state $\mathcal{U}_2$ is stable, and it is unstable for $\mathcal{R}_0 > 1$.*

Remark 2. *The vector-free equilibrium $\mathcal{U}_1$ is stable if $bme^{-c\tau} - c(m + c) < 0$ holds, while $\mathcal{U}_2$ exists provided $bme^{-c\tau} - c(m + c) > 0$. This means that the disease-free equilibrium is feasible only when the vector-free equilibrium is unstable.*

3.4. Stability of the endemic equilibrium

Following the stability of the disease-free equilibrium, we consider two different cases: Case I with $\tau = 0$, and Case II, when $\tau > 0$.

Case I. When $\tau = 0$, the characteristic equation associated with the endemic steady state $\mathcal{U}^*$ simplifies to a quintic form:

$$\xi^5 + \sigma_1\xi^4 + (\sigma_2 + \sigma_6)\xi^3 + (\sigma_3 + \sigma_7)\xi^2 + (\sigma_4 + \sigma_8)\xi + (\sigma_5 + \sigma_9) = 0.$$

We introduce new parameters $\mu_1 = \sigma_1$, $\mu_2 = \sigma_2 + \sigma_6$, $\mu_3 = \sigma_3 + \sigma_7$, $\mu_4 = \sigma_4 + \sigma_8$, $\mu_5 = \sigma_5 + \sigma_9$. The Routh-Hurwitz criterion requires all eigenvalues to be negative, or to possess negative real parts, if the following constraints are met:

$$\begin{aligned} &\mu_5 > 0,\ \mu_1\mu_2 - \mu_3 > 0,\ \mu_3(\mu_1\mu_2 - \mu_3) - \mu_1(\mu_1\mu_4 - \mu_5) > 0, \\ &(\mu_1\mu_2 - \mu_3)(\mu_3\mu_4 - \mu_2\mu_5) + (\mu_1\mu_4 - \mu_5)(\mu_5 - \mu_1\mu_4) > 0. \end{aligned} \tag{20}$$

Given that the steady state $\mathcal{U}^*$ is contingent upon several model parameters, we use $\theta \in \mathbb{R}$ as a general bifurcation parameter to assess the potential for Hopf bifurcation, leading to the following conclusion.

Theorem 3. *The endemic steady state $\mathcal{U}^*$ stays stable if the Routh–Hurwitz criteria (20) are satisfied. When $\theta = \theta^*$, the steady state $\mathcal{U}^*$ may become unstable and induce a Hopf bifurcation, contingent upon the fulfillment of one of the set criteria:*

i. $\phi(\theta^*) = 0$ *and* $\left.\dfrac{d\phi}{d\theta}\right|_{\theta=\theta^*} \neq 0$, *where*

$$\phi(\theta) = (\mu_3 - \mu_1\mu_2)(\mu_5\mu_2 - \mu_3\mu_4) - (\mu_5 - \mu_1\mu_4)^2,$$

with

$$\varphi = \frac{\mu_5 - \mu_1\mu_4}{\mu_3 - \mu_1\mu_2} > 0, \quad \mu_3 - \mu_1\varphi \neq 0;$$

ii. $\mu_5 = \mu_1\mu_4$, $\mu_3 = \mu_1\mu_2$, $\mu_4 < 0$, $\mu_1\mu_3 \neq 0$;

$$\left[\mu_1'^2 + (\mu_1\mu_2' - \mu_3')\varphi - (\mu_1\mu_4' - \mu_5')\right]\Big|_{\theta=\theta^*} \neq 0,$$

where μ_i', $i = 1, \ldots, 5$, *denote the derivatives of* μ_i *with respect to the bifurcation parameter* θ, *and*

$$\varphi = \frac{1}{2}\left(\mu_2 + \sqrt{\mu_2^2 - 4\mu_4}\right) > 0.$$

The proof of this theorem follows from some earlier work [5, 30]. In the next section, we will conduct numerical simulations to examine the impact of varying parameters on the stability of the endemic steady state.

Case II. For $\tau > 0$, the corresponding characteristic equation takes the form

$$\psi(\xi, \tau) = \left(\xi^5 + \sigma_1\xi^4 + \sigma_2\xi^3 + \sigma_3\xi^2 + \sigma_4\xi + \sigma_5\right) + e^{-\xi\tau}\left(\sigma_6\xi^3 + \sigma_7\xi^2 + \sigma_8\xi + \sigma_9\right) = 0. \tag{21}$$

The roots of (21) are contingent upon τ, and a Hopf bifurcation may take place, provided these roots can move along the imaginary axis with non-zero speed, leading to a stability transition for the endemic stable state. To investigate the potential for Hopf bifurcation, we examine a scenario in which the characteristic Eq (21) has a pair of purely imaginary roots, $\pm i\eta$, where $\eta > 0$. Substituting this into Eq (21) and separating real and imaginary parts gives

$$\begin{aligned} \sigma_1\eta^4 - \sigma_3\eta^2 + \sigma_5 &= -\left(-\sigma_7\eta^2 + \sigma_9\right)\cos\eta\tau - \left(-\sigma_6\eta^3 + \sigma_8\eta\right)\sin\eta\tau, \\ \eta^5 - \sigma_2\eta^3 + \sigma_4\eta &= -\left(-\sigma_6\eta^3 + \sigma_8\eta\right)\cos\eta\tau + \left(\sigma_4\eta^4 - \sigma_2\eta^2 + \sigma_9\right)\sin\eta\tau. \end{aligned} \tag{22}$$

These equations are combined by adding their squares together, which results in the next algebraic equation for η:

$$\eta^{10} + m_1\eta^8 + m_2\eta^6 + m_3\eta^4 + m_4\eta^2 + m_5 = 0, \tag{23}$$

where

$$\begin{aligned} &m_1 = \sigma_1^2 - 2\sigma_2, \quad m_2 = \sigma_2^2 - \sigma_6^2 - 2\sigma_1\sigma_3 + 2\sigma_4, \\ &m_3 = \sigma_3^2 - \sigma_7^2 + 2\sigma_6\sigma_8 - 2\sigma_2\sigma_4 + 2\sigma_1\sigma_5, \\ &m_4 = k_6^2k_1^2 - 2\sigma_3\sigma_5 + 2\sigma_7\sigma_9, \quad m_5 = \sigma_5^2 - \sigma_9^2. \end{aligned} \tag{24}$$

Introducing an auxiliary variable $z = \eta^2$, this equation can be rewritten in the form

$$h(z) = z^5 + m_1z^4 + m_2z^3 + m_3z^2 + m_4z + m_5 = 0. \tag{25}$$

Differentiating the function $h(z)$ gives

$$\frac{dh}{dz} = 5z^4 + 4m_1z^3 + 3m_2z^2 + 2m_3z + m_4. \tag{26}$$

Lemma 1. *If* $m_5 < 0$, *then Eq (25) will have at least one real positive root.*

Proof. Since $h(0) = m_5$ and $\lim_{z\to\infty} h(z) = \infty$, due to $h(z)$ being a continuous function, if $m_5 < 0$, then the intermediate value theorem shows that there exists at least one positive root $z_0 \in (0, \infty)$ of $h(z) = 0$. □

For any such positive root z_0, the characteristic Eq (21) will have a pair of purely imaginary roots $\pm i\xi_0 = \pm i\sqrt{z_0}$ for that particular value τ_0 of the time delay τ, as determined by system (22). Assuming no loss of generality, consider that Eq (25) possesses five distinct, real, and positive roots, denoted by z_1, z_2, z_3, z_4, and z_5. In this case, Eq (23) possesses positive roots, namely, $\eta_i = \sqrt{z_i}$, $i = 1, \ldots, 5$, and for each particular value of τ_i that corresponds to η_i, Eq (21) has a pair of purely imaginary roots, namely, $\pm i\eta_i$.

For every η_k, $k = 1, \ldots, 5$, the corresponding critical value of time delay is

$$\tau_k^j = \frac{1}{\eta_k}\Big[\arccos\Big(-\frac{\sigma_6\eta_k^8 + (\sigma_8 - \sigma_7\sigma_1 + \sigma_6\sigma_2)\eta_k^6 + (\sigma_9\sigma_1 - \sigma_8\sigma_2 + \sigma_7\sigma_3 - \sigma_6\sigma_4)\eta_k^4}{(-\sigma_7\eta_k^2 + \sigma_9)^2 + (-\sigma_6\eta_k^3 + \sigma_8\eta_k)^2} - \frac{(-\sigma_9\sigma_3 + \sigma_8\sigma_4 - \sigma_7\sigma_5)\eta_k^2 + \sigma_9\sigma_5}{(-\sigma_7\eta_k^2 + \sigma_9)^2 + (-\sigma_6\eta_k^3 + \sigma_8\eta_k)^2}\Big) + 2\pi j\Big],\ j = 0, 1, 2, ... \tag{27}$$

Let, $\tau_0 = \min\{\tau_{k_0}^0\}$, $\eta_0 = \eta_{k_0}$, $k_0 \in \{1, \ldots, 5\}$. Differentiating (21) with respect to τ gives

$$\left(\frac{d\xi}{d\tau}\right)^{-1} = \frac{(5\xi^4 + 4\sigma_1\xi^3 + 3\sigma_2\xi^2 + 2\sigma_3\xi + \sigma_4)e^{\xi\tau} + (3\sigma_6\xi^2 + 2\sigma_7\xi + \sigma_8)}{\sigma_6\xi^3 + \sigma_7\xi^2 + \sigma_8\xi + \sigma_9} - \frac{\tau}{\xi}, \tag{28}$$

and hence, we find

$$\mathrm{Re}\left(\frac{d\xi}{d\tau}\Big|_{\tau=\tau_0}\right)^{-1} = \frac{P_1P_2 + Q_1Q_2}{(P_2)^2 + (Q_2)^2}, \tag{29}$$

where

$$\begin{aligned}
P_1 &= 5\eta_0^4\sin(\eta_0\tau_0) + [-4\sigma_1\cos(\eta_0\tau_0) + \sigma_6\tau_0]\eta_0^3 \\
&\quad - 3\sigma_2\eta_0^2\sin(\eta_0\tau_0) + [2\sigma_7 + 2\sigma_3\cos(\eta_0\tau_0) - \sigma_8\tau_0]\eta_0 + \sigma_4\sin(\eta_0\tau_0), \\
Q_1 &= [-5\cos(\eta_0\tau_0)]\eta_0^4 - 4\sigma_1\eta_0^3\sin(\eta_0\tau_0) + [\sigma_7\tau_0 + 3\sigma_2\cos(\eta_0\tau_0)]\eta_0^2 \\
&\quad + 2\sigma_3\eta_0\sin(\eta_0\tau_0) - \sigma_4\cos(\eta_0\tau_0) - \sigma_8 + \sigma_9\tau_0, \\
P_2 &= -\sigma_7\eta_0^3 + \sigma_9\eta_0, \quad Q_2 = -\sigma_6\eta_0^4 + \sigma_8\eta_0^2.
\end{aligned}$$

Now, if the condition $P_1P_2 + Q_1Q_2 \neq 0$ holds, then the transversality condition $\mathrm{Re}\left(\frac{d\xi}{d\tau}|_{\tau=\tau_0}\right)^{-1} \neq 0$ is satisfied. Consequently, in light of the aforementioned findings and the Hopf bifurcation theorems about functional differential equations [31, 32], we provide the following result.

Theorem 4. *If conditions $\mathcal{R}_0 > 1$ and $\mu_i > 0$ are satisfied for all $i = 1, 2, ..., 5$, then for the endemic steady state $\mathcal{U}^*$ of model (2), the following conclusions are true:*

(i) $\mathcal{U}^*$ remains locally asymptotically stable for all $\tau \geq 0$ if $m_i > 0$, where $i = 1, \ldots, 5$.

(ii) If $m_5 < 0$ and $P_1P_2 + Q_1Q_2 \neq 0$, then $\mathcal{U}^*$ is locally asymptotically stable for $\tau \in [0, \tau_0)$ and unstable for $\tau > \tau_0$. When $\tau = \tau_0$, $\mathcal{U}^*$ undergoes Hopf bifurcation.

Remark 3. *Theorem 4 holds true provided that Eq (23) admits at least one positive real root, a condition that guarantees this is when $m_5 < 0$.*

4. Sensitivity analysis

Here, we analyze the local and global sensitivities of the parameters.

4.1. Sensitivity analysis using $\mathcal{R}_0$

To investigate the effect of individual parameters on the basic reproduction number ($\mathcal{R}_0$), we first conducted a local sensitivity analysis. Using the normalized forward sensitivity index, we derived explicit expressions for the impact of each parameter ς on $\mathcal{R}_0$ using the relation $\chi_\varsigma = \frac{\varsigma}{\mathcal{R}_0} \cdot \frac{\partial \mathcal{R}_0}{\partial \varsigma}$, and we get

$$\begin{cases} \varkappa_a = 0.5, \ \varkappa_K = 1, \quad \varkappa_b = \dfrac{1}{2}\dfrac{c(m+c)}{bme^{-c\tau} - c(m+c)}, \\ \varkappa_m = \dfrac{1}{2}\dfrac{\left((bme^{-c\tau} - c\,(m+c)) + c^2 + me^{-c\tau}c\right)c}{(c+me^{-c\tau})\,(bme^{-c\tau} - c\,(m+c))}, \\ \varkappa_c = -\dfrac{1}{2}\dfrac{e^{-c\tau}mc\,(c\tau+1)\,(m+b+c) + e^{-c\tau}c^2m + c^3 + (c+me^{-c\tau})\,(bme^{-c\tau} - c\,(m+c))}{(c+me^{-c\tau})\,(bme^{-c\tau} - c\,(m+c))}, \\ \varkappa_\tau = -\dfrac{1}{2}\dfrac{(m+b+c)e^{-c\tau}mc^2\tau}{(c+me^{-c\tau})\,(bme^{-c\tau} - c\,(m+c))}, \ \ \varkappa_\lambda = \varkappa_\beta = \dfrac{1}{2}, \ \varkappa_\alpha = -\dfrac{1}{2}, \end{cases} \tag{30}$$

where $bme^{-c\tau} - c(m+c) > 0$. Equation (30) shows that parameters a, K, b, m, λ, and β have a positive influence, while c, τ, and α have a negative influence. These findings indicate that reducing a, K, b, m, λ, and β or enhancing c, τ, and α significantly reduce infection transmission.

For the purpose of numerical simulation, we use the values of the parameters as in Table 1 and pick $\tau = 5$. The sensitivity indices of the model parameters are illustrated in Figure 1, with a detailed summary provided in Table 2. A 10% alteration in the carrying capacity K produces an approximate 10% change in the basic reproduction number $\mathcal{R}_0$. In contrast, a 10% increase in the vector maturation period τ yields an estimated 2.51% decrease in $\mathcal{R}_0$. The remaining parameters display consistent patterns of influence and can be analyzed in the same manner as K and τ to determine their respective effects on $\mathcal{R}_0$.

Table 1. Parameters of model (2) and their baseline values [27, 28].

Parameter	Brief description	Value (unit)
r	susceptible plant growth rate	0.03 day^{-1}
K	carrying capacity of a plantation	1 m^{-2}
λ	rate of infection transmission in plants	0.0025 vector^{-1} day^{-1}
b	the rate at which the vector population reproduces	0.5 day^{-1}
α	the plant mortality rate	0.03 day^{-1}
β	the vector-mediated infection transmission rate	0.032 plant^{-1}day^{-1}
a	vector abundance on a plant	300 plant^{-1}
c	mortality rate of vector	0.06 day^{-1}
m	maturation rate of vector	0.03 day^{-1}

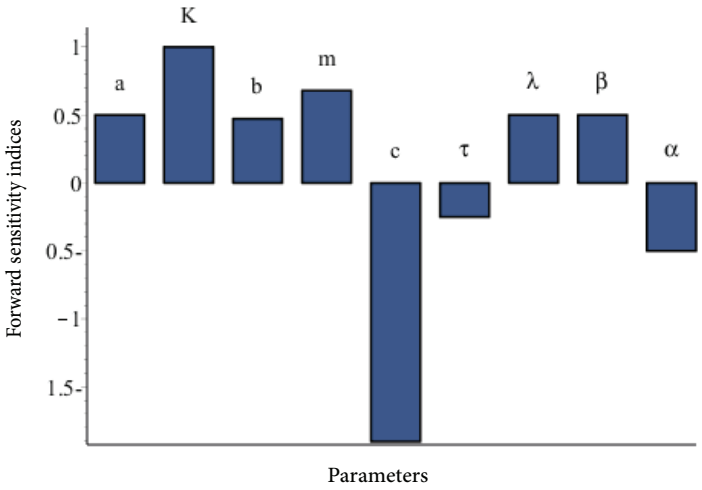

Figure 1. Forward sensitivity analysis using $\mathcal{R}_0$.

Table 2. Sensitivity indices of the parameters with respect to $\mathcal{R}_0$ of system (2).

Parameter	Sensitivity	Parameter	Sensitivity	Parameter	Sensitivity
a	0.5	m	0.67997	λ	0.5
K	1	c	−1.90389	β	0.5
b	0.47267	τ	−0.25126	α	−0.5

4.2. Sensitivity of parameters using a model population

In this section, we conduct a sensitivity analysis of the parameters that regulate system (2), following the methodological framework proposed by Saltelli et al. [33, 34]. This technique facilitates the identification of the most influential parameters affecting the system dynamics. Assessing how the model reacts to small variations in these parameters is crucial for validating its robustness and ensuring dependable predictive performance.

Figure 2 presents the results of the sensitivity analysis, showcasing how the partial derivatives of each population variable evolve over time in response to changes in their respective parameters. To assess the forward or direct sensitivity of a given parameter ζ with respect to a population variable w, we examine the time-dependent behavior of $\partial w/\partial\zeta$. This analysis is implemented computationally using the ode45 solver in MATLAB R2016a (OS: Windows 10 Pro, 64-bit Intel(R) Core(TM) i5-3570 CPU @ 3.40GHz, 8GB RAM; Relative Tolerance (RelTol) = 10^{-6}, Absolute Tolerance (AbsTol) = 10^{-8}), which streamlines the process by extending the original system of ordinary differential equations (ODEs) with a set of auxiliary equations. These equations are obtained by differentiating the original system with respect to each parameter, allowing for the concurrent integration of both the system dynamics and their associated sensitivities.

Certain parameters, such as the infection rate λ and maturation rate m, exhibit positive sensitivity with respect to the population of infected plants. This shows that increases in the values of these parameters enhance the level of infection. In contrast, parameters like plant mortality rate α and vector mortality rate c demonstrate negative sensitivity, suggesting that higher values contribute to a reduction

in the infected plant population.

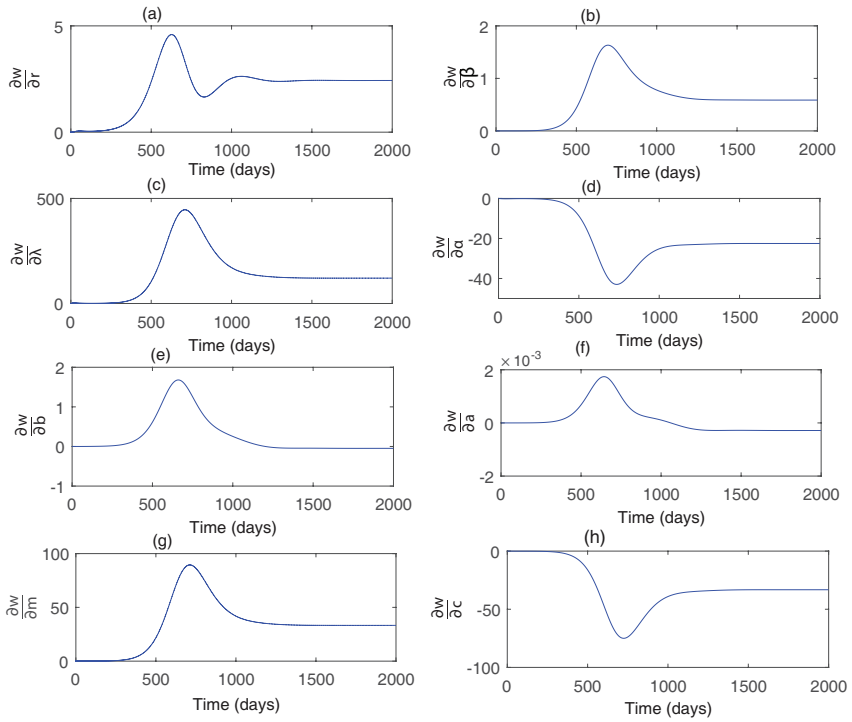

Figure 2. Sensitivity of the parameters of model (2) with respect to the infected plant population w for $\tau = 0$.

5. Numerical stability and simulations

Numerical stability, bifurcation analyses, and simulations are conducted in this section to investigate the impact of various parameters on the dynamics of the system and to illustrate the different regimes that can be observed in the model. The baseline values of the parameters are provided in Table 1.

Figure 3 demonstrates how the basic reproduction number $\mathcal{R}_0$ varies in response to changes in the vector maturation period τ, the reproduction rate b, and the transmission rate β from infected plants to susceptible mature vectors. When $\mathcal{R}_0$ falls below 1, the system gradually eliminates infected plants and vectors, ultimately settling at the disease-free equilibrium $\mathcal{U}_2$. However, when the basic reproduction number $\mathcal{R}_0$ approaches unity, this equilibrium becomes unstable due to forward transcritical bifurcation, leading to the emergence of an endemic equilibrium $\mathcal{U}^*$. For values of $\mathcal{R}_0$ exceeding 1, the disease-free state becomes unstable. The figure further reveals that when the transmission rate β is sufficiently low, the disease-free state remains stable regardless of the maturation period τ. In such cases, the infection is eliminated more rapidly than it can propagate, irrespective of how quickly vectors mature. However, as β increases, stability of the disease-free state is only maintained if τ is large enough to delay the maturation and reproduction of vectors, thereby slowing the spread of infection. There exists a threshold value of τ beyond which the disease-free equilibrium becomes biologically unfeasible. This occurs because the rate at which new immature vectors are produced fails to compensate for vector mortality. A similar outcome is observed when the reproduction rate b is too low under these conditions, the vector population cannot sustain itself, and

the disease-free state ceases to exist for any value of τ. For intermediate values of τ, the disease-free equilibrium remains stable only when both β and b are relatively low; otherwise, the system transitions to an endemic situation.

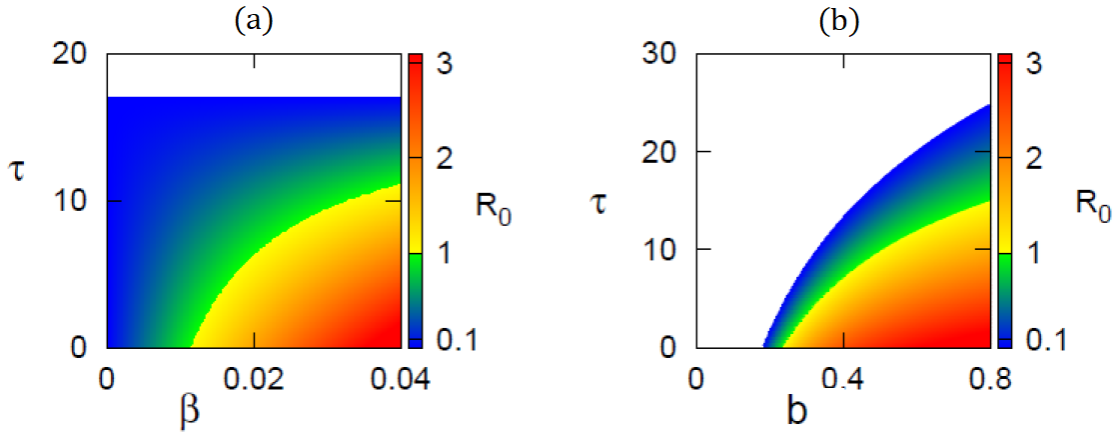

Figure 3. Areas of stability for the disease-free steady state $\mathcal{U}_2$. The stability of $\mathcal{U}_2$ is observed when $\mathcal{R}_0 < 1$, whereas it becomes unstable when $\mathcal{R}_0 > 1$. The values of the parameters are derived from Table 1. In the white region, the steady state $\mathcal{U}_2$ is infeasible, while the vector-free steady state $\mathcal{U}_1$ demonstrates stability.

In the scenario where maturation occurs instantaneously ($\tau = 0$), Figure 4 illustrates the emergence of a stable endemic equilibrium $\mathcal{U}^*$ as the basic reproduction number $\mathcal{R}_0$ reaches unity. With an increase in the maturation rate m, the endemic equilibrium $\mathcal{U}^*$ undergoes a Hopf bifurcation, resulting in the emergence of persistent periodic oscillations around this state.

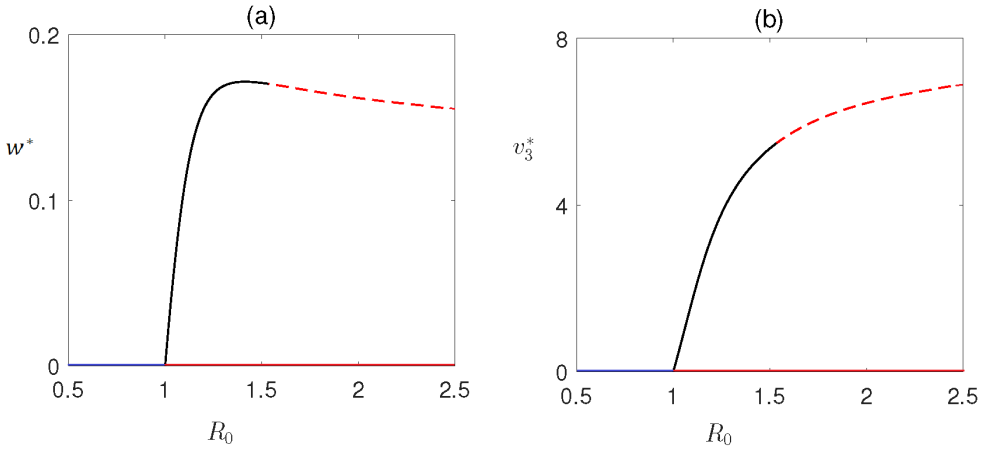

Figure 4. Bifurcation diagram with $\mathcal{R}_0$ as the bifurcation parameter plotted by varying the maturation rate, m. The values of the parameters are derived from Table 1, and $\tau = 0$. Disease-free equilibrium $\mathcal{U}_2$ is stable when $\mathcal{R}_0 < 1$ (blue lines) and unstable otherwise (red lines). At $\mathcal{R}_0 = 1$, endemic equilibrium $\mathcal{U}^*$ becomes feasible, and for sufficiently small values of $\mathcal{R}_0 > 1$, it is stable (black solid lines), but then loses stability as the value of $\mathcal{R}_0$ increases (red dashed lines).

Figure 5 captures the dynamics associated with this transition. For lower values of m, the system exhibits damped oscillations that converge to the steady state $\mathcal{U}^*$, consistent with the result stated in Theorem 3. Beyond the bifurcation point, the system shifts to a regime of persistent oscillatory behavior. Further insights are provided in Figure 6, which displays how the amplitude—represented by the minima and maxima of these periodic solutions—varies as the maturation rate m changes.

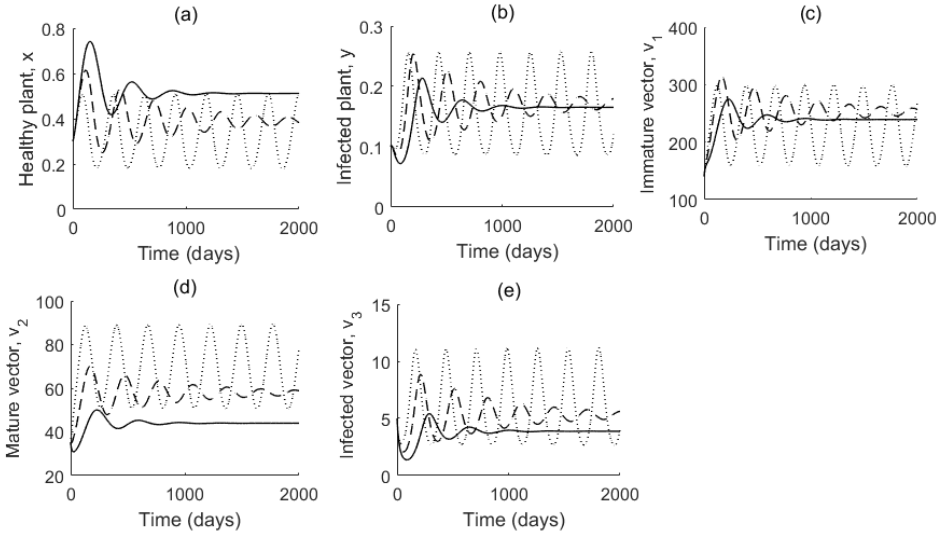

Figure 5. Numerical solutions of system (2) with parameter values from Table 1, when $\tau = 0$, for different values of m: $m = 0.012$ (solid lines), $m = 0.015$ (dashed lines), and $m = 0.02$ (dotted lines).

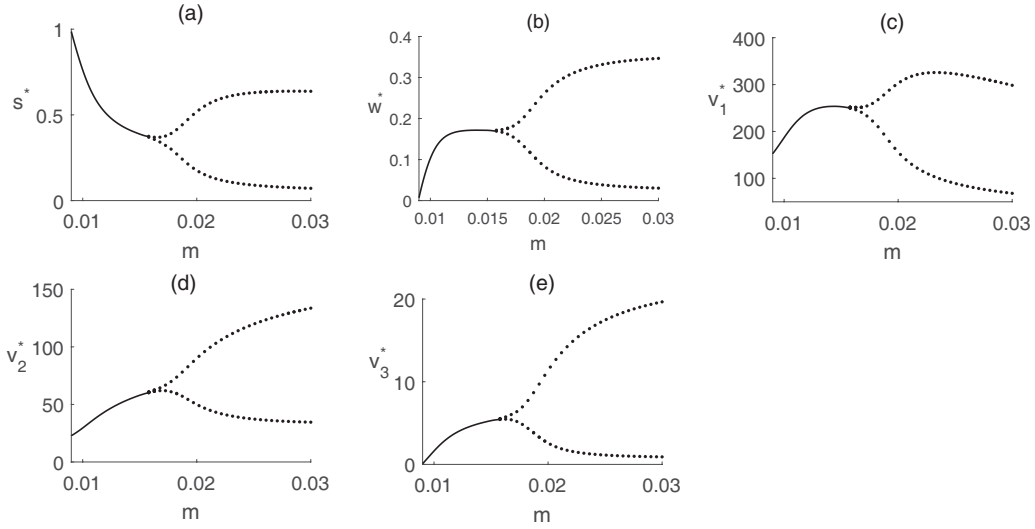

Figure 6. Bifurcation diagram using the maturation rate m as the bifurcation parameter, with all other parameters taken from Table 1 and delay $\tau = 0$. The dotted lines represent the maximum and minimum values of periodic trajectories surrounding the endemic steady state $\mathcal{U}^*$.

Continuing with the scenario of instantaneous maturation ($\tau = 0$), Figure 7 depicts the stability regions of various steady states as influenced by the vector maturation rate m, the transmission rate λ from infected vectors to susceptible plants, and the transmission rate β from infected plants to uninfected adult vectors. The stability patterns for λ and β are notably similar. When m is sufficiently low, the system consistently stabilizes at the vector-free equilibrium $\mathcal{U}_1$, regardless of the values of λ or β.

As m increases, a transition occurs with the appearance of the disease-free equilibrium $\mathcal{U}_2$, which remains stable under lower values of λ or β. However, as either transmission rate rises, $\mathcal{U}_2$ loses stability, giving way to a stable endemic equilibrium $\mathcal{U}^*$. At high values of both m and the transmission rates, the system further evolves into a regime characterized by stable periodic oscillations around $\mathcal{U}^*$.

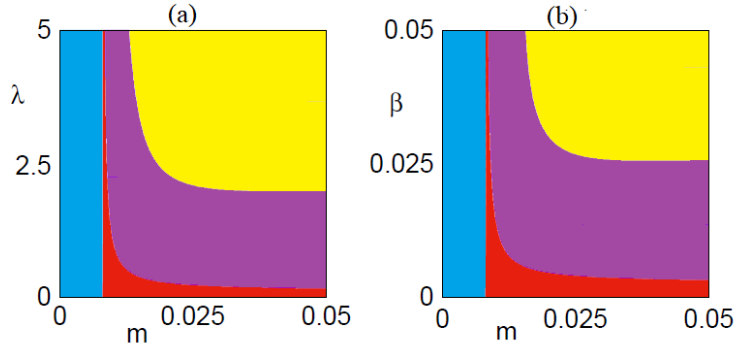

Figure 7. Stability zones for various steady states of system (2) are illustrated using the parameters listed in Table 1, with $\tau = 0$. The sky-blue area indicates where the axial vector-free equilibrium $\mathcal{U}_1$ remains stable. The red region corresponds to the stability of the disease-free state $\mathcal{U}_2$. The endemic equilibrium $\mathcal{U}^*$ is stable within the violet zone and becomes unstable in the yellow region.

The influence of the vector maturation period τ on system dynamics is depicted in Figure 8, which presents numerical simulations across various τ values. In the case of instantaneous maturation ($\tau = 0$), the system demonstrates stable, recurring oscillations surrounding the endemic equilibrium $\mathcal{U}^*$. However, as τ increases, these oscillations vanish through an inverse supercritical Hopf bifurcation, leading to the stabilization of $\mathcal{U}^*$. Further increases in τ result in damped oscillatory behavior, with solutions gradually settling into the endemic steady state.

Figure 9 offers additional insight by tracking the peaks and troughs of the periodic solutions around $\mathcal{U}^*$, when present. As τ increases, the equilibrium levels of all state variables generally decrease in a monotonic fashion, with the exception of the susceptible plant population, which consistently rises.

Figure 10 illustrates how the system evolves toward different long-term states based on variations in the vector maturation period τ, the disease transmission rate from vectors to plants λ, and the vector maturation rate m. For sufficiently large values of τ, the system gravitates toward the stable vector-free equilibrium $\mathcal{U}_1$, since delayed maturation and reproduction hinder the formation of a viable vector population. If all parameters are held constant except for λ, there exists a threshold value of τ, independent of λ, beyond which the system consistently converges to the vector-free state $\mathcal{U}_1$. However, when τ falls below this threshold, increasing λ triggers a progression of dynamic shifts: first from the disease-free equilibrium $\mathcal{U}_1$ to an endemic steady state $\mathcal{U}^*$, and then to oscillatory behavior

around $\mathcal{U}^*$.

A similar pattern emerges when the maturation rate m is increased. For any fixed value of λ or m, raising τ causes the periodic oscillations around $\mathcal{U}^*$ to vanish, leading the system to stabilize at $\mathcal{U}^*$, then transition to a disease-free equilibrium $\mathcal{U}_2$, and ultimately return to the vector-free state $\mathcal{U}_1$.

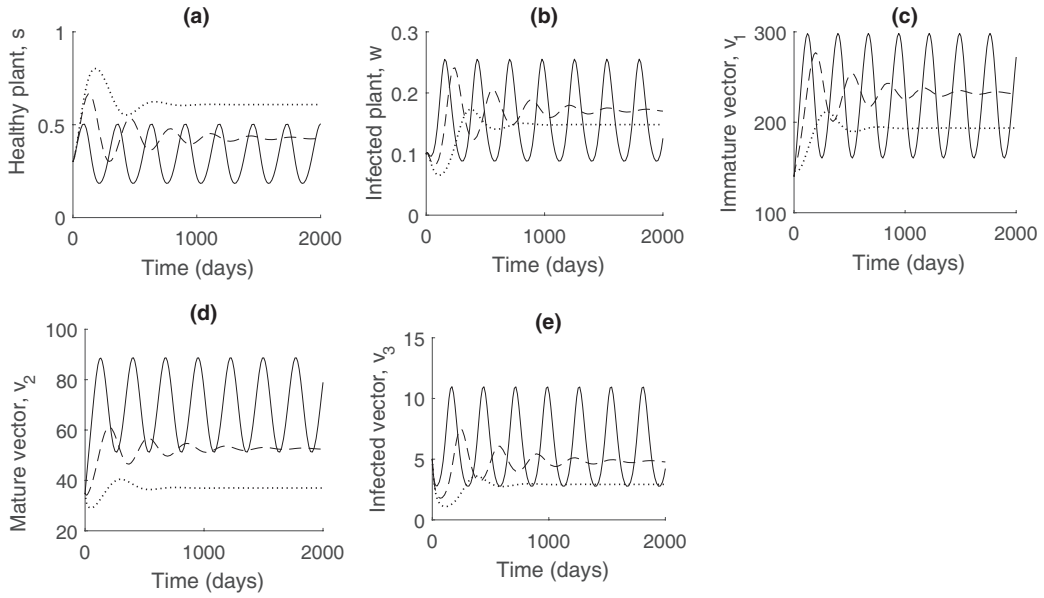

Figure 8. Numerical solution of system (2) with $m = 0.03$ and other parameters from Table 1, as well as $\tau = 0$ (solid line), $\tau = 5$ (dashed line), $\tau = 10$ (dotted line).

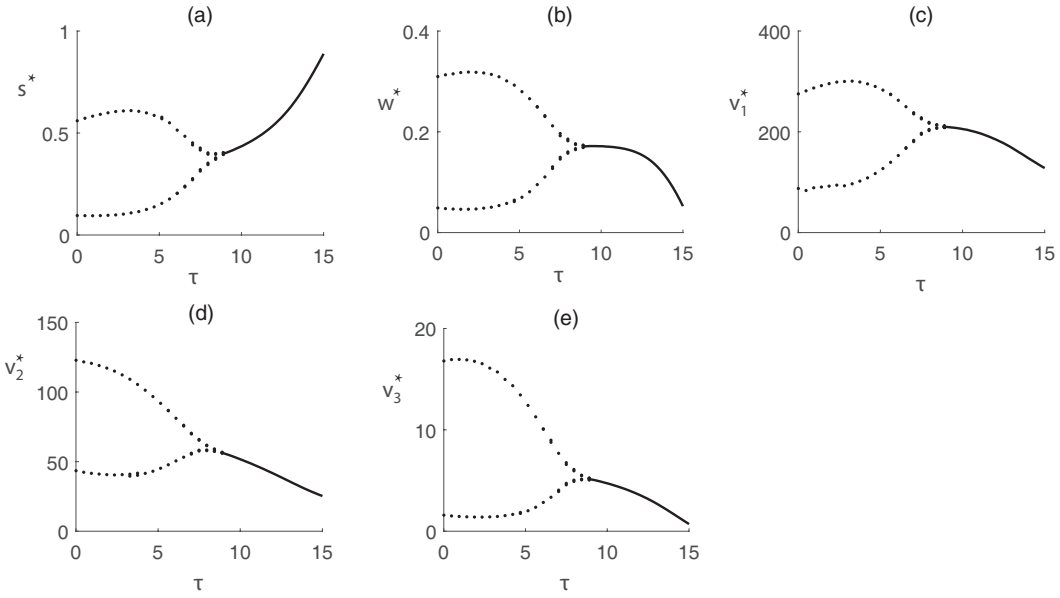

Figure 9. Bifurcation diagram illustrating the role of τ (maturation time) as the bifurcation parameter, with all other parameters set according to Table 1. The plotted dots represent the minima and maxima of periodic solutions surrounding the endemic steady state $\mathcal{U}^*$.

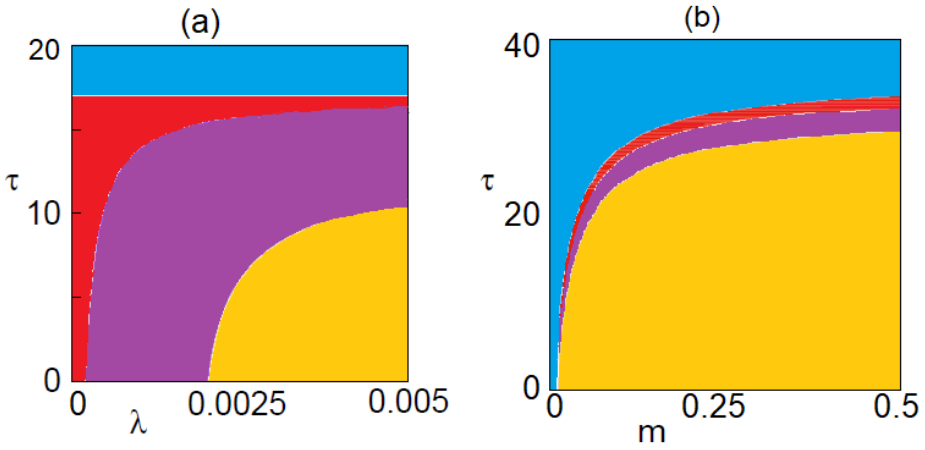

Figure 10. Stability regions of system (2) based on parameter values from Table 1. The sky-blue area indicates stability of the axial vector-free equilibrium $\mathcal{U}_1$, while the red region corresponds to the stable disease-free state $\mathcal{U}_2$. The endemic equilibrium $\mathcal{U}^*$ is stable within the violet region and becomes unstable in the yellow zone.

6. Conclusions

To investigate the behavior of plant viral infections transmitted by vectors, this study introduces a stage-structured mathematical model that incorporates stages of the vector and a time delay representing the maturation period of the vector. A key focus is the basic reproduction number, denoted as $\mathcal{R}_0$, which determines whether the infection will die out, leading to a stable disease-free equilibrium when $\mathcal{R}_0 < 1$, or persist, resulting in an endemic steady state. In the endemic system, the infection either stabilizes at a constant level when the endemic equilibrium $\mathcal{U}^*$ is stable or fluctuates periodically around $\mathcal{U}^*$.

This study reveals that extending the vector maturation delay τ tends to lower $\mathcal{R}_0$, thereby promoting the eradication of the infection. When both the maturation delay and the maturation rate m are relatively small, increasing the maturation rate m can push the system past the critical threshold $\mathcal{R}_0 = 1$, leading to the establishment of a stable endemic state $\mathcal{U}^*$. Nevertheless, this stable state can be disrupted via a Hopf bifurcation, leading to persistent oscillatory dynamics in the population levels. Conversely, if the value of m is not too low, the system may exhibit persistent oscillations around $\mathcal{U}^*$ even when the maturation delay τ is negligible. In such cases, increasing τ can suppress these oscillations via an inverse supercritical Hopf bifurcation, ultimately stabilizing the endemic equilibrium $\mathcal{U}^*$.

The findings of this study indicate that the time delay associated with vector maturation does not necessarily result in destabilization of the system's steady states. On the contrary, under certain conditions, particularly when smaller delays correspond to periodic fluctuations, increasing the maturation period can actually suppress oscillations in both vector and plant populations and stabilize the endemic equilibrium. This phenomenon is similar to a situation we analyzed earlier in a model of vector-plant disease without a stage structure, where increasing the period of latency was also associated with the stabilization of the endemic equilibrium [14]. Possible intuition behind this is an observation that while infected plants are causing new infections in mature vectors, it is mature infected vectors that cause new infections in susceptible plants, but to facilitate this cycle of

exchange of infection between plant and vector populations, there is a need for all processes to take place on a certain timescale. In this respect, a longer maturation period effectively slows down the cycle for vectors of going through being susceptible, then maturing, then acquiring infection from infected plants, becoming themselves infected, and causing new infections in plants. Hence, by virtue of this slowdown in vector dynamics, the continuous cycle of mutual infection stops, and both vector and plant populations instead settle on some steady levels. Interestingly, our numerical bifurcation analysis showed that increasing the value of the maturation period τ corresponds to lower values of all state variables at the steady state $\mathcal{U}^*$ except for the susceptible plant population, suggesting that while longer maturation is detrimental to vectors, it is actually beneficial to plants.

The alteration of the maturation period in vectors presents significant challenges due to its basis in natural developmental biology. This period is typically influenced by genetic and environmental factors, making direct manipulation complex. However, in practical applications, such as vector control programs and laboratory-based genetic studies, finding ways to adjust this period is highly beneficial [35]. Our results could help biologists and pest control managers to explore methods such as environmental modulation (which involves adjusting temperature, humidity, or light cycles), gene editing, and chemical or hormonal treatments to either shorten or lengthen the maturation period of vectors [36]. Although these approaches are largely experimental, they, along with our findings, could be valuable for optimizing laboratory rearing protocols and reducing disease transmission windows in the field. Overall, our results not only provide a theoretical framework but also open new avenues for biologists and pest control managers to explore.

Author contributions

Aeshah A. Raezah: Methodology, validation, software, visualization; Konstantin B. Blyuss: Conceptualization, methodology, writing-original draft preparation, supervision; Selim Reja: Methodology, validation, software, visualization; Fahad Al Basir: Conceptualization, methodology, validation, software, writing-original draft preparation, supervision. All authors have read and agreed to publish the manuscript.

Use of Generative-AI tools declaration

The authors declare they have not used Artificial Intelligence (AI) tools in the creation of this article.

Acknowledgments

The authors extend their appreciation to the Deanship of Research and Graduate Studies at King Khalid University for funding this work through the Large Group Project under grant number (RGP.2/58/46).

Conflict of interest

The authors declare no conflict of interest.

References

1. P. A. Link, M. Fuchs, Transmission specificity of plant viruses by vectors, *J. Plant Pathol.*, **87** (2005), 153–165. Available from: https://www.jstor.org/stable/41998234.
2. V. Z. Graff, V. Brault, *Role of vector-transmission proteins*, In: Plant Virology Protocols, Methods in Molecular Biology, Humana Press, **451** (2008), 81–96. https://doi.org/10.1007/978-1-59745-102-4_6
3. A. E. Whitfield, B. W. Falk, D. Rotenberg, Insect vector-mediated transmission of plant viruses, *Virology*, **479** (2015), 278–289. https://doi.org/10.1016/j.virol.2015.03.026
4. H. Naveed, W. Islam, M. Jafir, V. Andoh, L. Chen, K. Chen, A review of interactions between plants and whitefly-transmitted begomoviruses, *Plants*, **12** (2023), 3677. https://doi.org/10.3390/plants12213677
5. F. A. Basir, K. B. Blyuss, S. Ray, Modelling the effects of awareness-based interventions to control the mosaic disease of Jatropha curcas, *Ecol. Complex.*, **36** (2018), 92–100. https://doi.org/10.1016/j.ecocom.2018.07.004
6. H. Czosnek, A. H. Shalev, I. Sobol, R. Gorovits, M. Ghanim, The incredible journey of begomoviruses in their whitefly vector, *Viruses*, **9** (2017), 273. https://doi.org/10.3390/v9100273
7. D. R. Jones, Plant viruses transmitted by whiteflies, *Eur. J. Plant Pathol.*, **109** (2003), 195–219. https://doi.org/10.1023/A:1022846630513
8. M. J. Jeger, J. Holt, F. V. D. Bosch, L. V. Madden, Epidemiology of insect-transmitted plant viruses: Modelling disease dynamics and control interventions, *Physiol. Entomol.*, **29** (2004), 291–304. https://doi.org/10.1111/j.0307-6962.2004.00394.x
9. D. Gerling, A. R. Horowitz, J. Baumgaertner, Autecology of Bemisia tabaci, *Agr. Ecosyst. Environ.*, **17** (1986), 5–19. https://doi.org/10.1016/0167-8809(86)90022-8
10. J. Salas, O. Mendoza, Biology of the sweetpotato whitefly (Homoptera: Aleyrodidae) on tomato, *Fla. Entomol.*, **78** (1995), 154–160. https://doi.org/10.2307/3495680
11. N. S. Butter, *Insect vectors and plant pathogens*, CRC Press, 2018. https://doi.org/10.1201/9780429503641
12. M. Jackson, B. M. C. Charpentier, Modeling plant virus propagation with delays, *J. Comput. Appl. Math.*, **309** (2017), 611–621. https://doi.org/10.1016/j.cam.2016.04.024
13. Q. Li, Y. Dai, X. Guo, X. Zhang, Hopf bifurcation analysis for a model of plant virus propagation with two delays, *Adv. Differ. Equ.*, **2018** (2018), 259. https://doi.org/10.1186/s13662-018-1714-8
14. F. A. Basir, K. B. Blyuss, E. Venturino, Stability and bifurcation analysis of a multi-delay model for mosaic disease transmission, *AIMS Math.*, **8** (2023), 24545–24567. https://doi.org/10.3934/math.20231252
15. F. A. Basir, Y. N. Kyrychko, K. B. Blyuss, S. Ray, Effects of vector maturation time on the dynamics of cassava mosaic disease, *B. Math. Biol.*, **83** (2021), 87. https://doi.org/10.1007/s11538-021-00921-4

16. A. Uke, H. Tokunaga, Y. Utsumi, N. A. Vu, P. T. Nhan, P. Srean, et al., Cassava mosaic disease and its management in Southeast Asia, *Plant Mol. Biol.*, **109** (2022), 301–311. https://doi.org/10.1007/s11103-021-01168-2

17. J. P. Legg, *African cassava mosaic disease*, In: Encyclopedia of Virology, 3 Eds., Academic Press, 2008, 30–36. https://doi.org/10.1016/B978-012374410-4.00693-2

18. B. Erick, M. Mayengo, Modelling the dynamics of cassava mosaic disease with non-cassava host plants, *Inform. Med. Unlocked*, **33** (2022), 101086. https://doi.org/10.1016/j.imu.2022.101086

19. M. Banerjee, Y. Takeuchi, Maturation delay for the predators can enhance stable coexistence for a class of prey-predator models, *J. Theor. Biol.*, **412** (2017), 154–171. https://doi.org/10.1016/j.jtbi.2016.10.016

20. B. Buonomo, M. Cerasuolo, The effect of time delay in plant–pathogen interactions with host demography, *Math. Biosci. Eng.*, **12** (2015), 473–490. https://doi.org/10.3934/mbe.2015.12.473

21. J. E. V. D. Plank, *Plant diseases: Epidemics and control*, Academic Press, 1963.

22. K. L. Cooke, Stability analysis for a vector disease model, *Rocky Mt. J. Math.*, **9** (1979), 31–42. Available from: https://www.jstor.org/stable/44238836.

23. F. A. Basir, P. K. Roy, Dynamics of mosaic disease with roguing and delay in Jatropha curcas plantations, *J. Appl. Math. Comput.*, **58** (2018), 1–31. https://doi.org/10.1007/s12190-017-1131-2

24. Z. Wang, B. Hu, L. Zhu, J. Lin, M. Xu, D. Wang, Hopf bifurcation analysis for Parkinson oscillation with heterogeneous delays: A theoretical derivation and simulation analysis, *Commun. Nonlinear Sci.*, **114** (2022), 106614. https://doi.org/10.1016/j.cnsns.2022.106614

25. E. Venturino, P. K. Roy, F. A. Basir, A. Datta, A model for the control of the mosaic virus disease in Jatropha curcas plantations, *Energy Ecol. Environ.*, **1** (2016), 360–369. https://doi.org/10.1007/s40974-016-0033-8

26. F. A. Basir, Role of whitefly maturation period on mosaic disease propagation in Jatropha curcas plant, *Front. Appl. Math. Stat.*, **9** (2023), 1238497. https://doi.org/10.3389/fams.2023.1238497

27. S. Adhurya, F. A. Basir, S. Ray, Stage-structure model for the dynamics of whitefly transmitted plant viral disease: An optimal control approach, *Comput. Appl. Math.*, **41** (2022), 154. https://doi.org/10.1007/s40314-022-01864-9

28. J. Holt, M. J. Jeger, J. M. Thresh, G. W. O. Nape, An epidemiological model incorporating vector population dynamics applied to African cassava mosaic virus disease, *J. Appl. Ecol.*, **34** (1997), 793–806. https://doi.org/10.2307/2404924

29. P. V. D. Driessche, J. Watmough, Reproduction numbers and sub-threshold endemic steady states for compartmental models of disease transmission, *Math. Biosci.*, **180** (2002), 29–48. https://doi.org/10.1016/s0025-5564(02)00108-6

30. C. Douskos, P. Markellos, Complete coefficient criteria for five-dimensional Hopf bifurcations, with an application to economic dynamics, *J. Nonlinear Dyn.*, **2015** (2015), 278234. https://doi.org/10.1155/2015/278234

31. J. Hale, *Theory of functional differential equations*, New York: Springer, 1977. Available from: https://link.springer.com/book/10.1007/978-1-4612-9892-2.

32. B. D. Hassard, N. D. Kazarinoff, Y. H. Wan, *Theory and applications of Hopf bifurcation*, London Mathematical Society Lecture Note Series, UK, Cambridge: Cambridge University Press, **41** (1981). https://doi.org/10.1002/zamm.19820621221

33. A. Saltelli, M. Scott, The role of sensitivity analysis in the corroboration of models and its link to model structural and parametric uncertainty, *Reliab. Eng. Syst. Safe.*, **57** (1997), 1–4. Available from: `https://publications.jrc.ec.europa.eu/repository/handle/JRC14027`.

34. A. Saltelli, S. Tarantola, K. S. Chan, A quantitative model-independent method for global sensitivity analysis of model output, *Technometrics*, **41** (1999), 39–56. https://doi.org/10.1080/00401706.1999.10485594

35. A. C. Ukubuiwe, I. K. Olayemi, F. O. Arimoro, I. C. J. Omalu, B. M. Baba, C. C. Ukubuiwe, et al., Influence of rearing-water temperature on life stages' vector attributes, distribution and utilisation of metabolic reserves in Culex quinquefasciatus (Diptera: Culicidae): Implications for disease transmission and vector control, *J. Basic Appl. Zool.*, **79** (2018), 32. https://doi.org/10.1186/s41936-018-0045-3

36. C. C. Heu, F. M. McCullough, J. Luan, J. L. Rasgon, CRISPR-Cas9-based genome editing in the silverleaf whitefly (Bemisia tabaci), *CRISPR J.*, **3** (2020), 89–96. https://doi.org/10.1089/crispr.2019.0067

AIMS Press